

Journal of Applied Physics 122, 055301 (published online 2 August 2017)

## Quantum efficiency modeling for a thick back-illuminated astronomical CCD

D. E. Groom,\* S. Haque, S. E. Holland, and W. F. Kolbe

*Lawrence Berkeley National Laboratory, Berkeley, CA 94720, USA*

(Dated: August 10, 2017)

The quantum efficiency and reflectivity of thick, back-illuminated CCD's being fabricated at LBNL for astronomical applications are modeled and compared with experiment. The treatment differs from standard thin-film optics in that (a) absorption is permitted in any film, (b) the 200–500  $\mu\text{m}$  thick silicon substrate is considered as a thin film in order to observe the fringing behavior at long wavelengths, and (c) by using approximate boundary conditions, absorption in the surface films is separated from absorption in the substrate. For the quantum efficiency measurements the CCD's are normally operated as CCD's, usually at  $T = -140^\circ\text{C}$ , and at higher temperatures as photodiodes. They are mounted on mechanical substrates. Reflectivity is measured on air-backed wafer samples at room temperature. The agreement between model expectation and quantum efficiency measurement is in general satisfactory.

arXiv:1708.02928v1 [physics.app-ph] 9 Aug 2017

---

\* degroom@lbl.gov

## I. INTRODUCTION

Fully depleted thick back-illuminated p-channel charge-coupled devices (CCD's) developed at Lawrence Berkeley National Laboratory (LBNL) for astronomical applications have useful quantum efficiencies (QE's) extending into the near infrared (IR)[1, 2]. The response is limited to  $\lesssim 1100$  nm by the indirect bandgap of silicon. The QE typically falls to about 50% at 1000 nm, depending on the temperature and thickness of the CCD. Thicknesses range from 200 to 500  $\mu\text{m}$ . The temperature range of interest is  $-140^\circ\text{C}$  to  $20^\circ\text{C}$ . If  $T \gtrsim -100^\circ\text{C}$ , the QE is measured by operating the device as a photodiode. A highly schematic cross section of a typical back-illuminated LBNL CCD is shown in Fig. 1.

Modeling the response depends crucially on the complex refractive indices and thicknesses of the materials involved. Especially critical is the absorption coefficient  $\alpha(\lambda, T)$  of silicon as the indirect bandgap is approached. Most of the other indices also present special problems.

While the formalism presented here is applicable to any CCD, we specialize to the LBNL case. In these CCD's, a thin film (10–25 nm) of *in-situ* doped polysilicon (ISDP) is grown on the rear surface to serve as an ohmic contact. Absorption in this layer limits the blue response, particularly below 450 nm. Over the ISDP is an antireflective coating optimized for maximum transmission at desired wavelengths, particularly in the near-infrared.

This paper and the corresponding code grew out of work reported by Groom[3] in 1999. At that time the treatment of absorption in the ISDP and surface films was *ad hoc* at best. Absorption by an indium-tin oxide (ITO) film was neglected. ISDP absorption was poorly modeled, so that results below about 550 nm were uncertain.

Although oblique incidence with either  $\mathbf{E}$  and  $\mathbf{B}$  parallel to the surface is treated, oblique incidence is of relatively little importance, since even for the extreme case of an f1 system the incident  $\cos\theta_0$  is  $\geq 0.89$ , and the ray is “quickly straightened” by refraction into the high-index silicon ( $n = 3.7\text{--}4$ ).

The design constraints are daunting: As shown in Fig. 2, the absorption length in silicon ranges over four orders of magnitude in the useful wavelength region, from a few nm at the atmospheric cutoff near 320 nm to the thickness of the CCD, typically 250  $\mu\text{m}$ . At the blue end of the spectrum it is close to the thickness of the (absorptive) ISDP, while at the near-IR end the CCD approaches transparency, with multiple reflections producing fringes.

The analysis uses the standard transfer matrix formalism described in multiple sources, *e.g.* in Refs. 8–10. Some departures are made in addressing CCD-specific absorption issues:

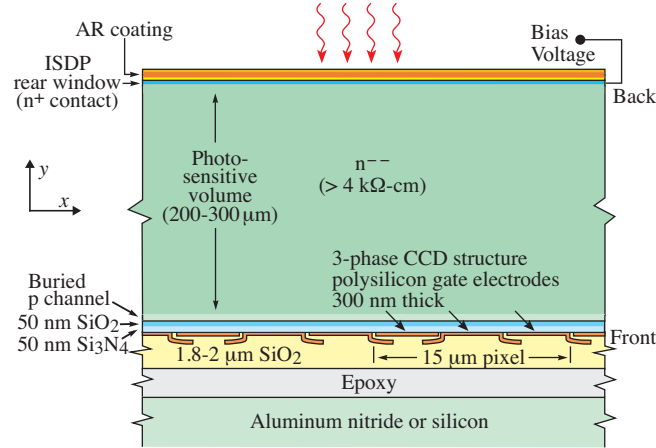


FIG. 1. Optical structure of the LBNL CCD. In different versions the substrate resistivity ranges from 4 to 20 k $\Omega$ -cm, and some of the CCD's have a 10.5  $\mu$ m pixel width. *Not to scale.*

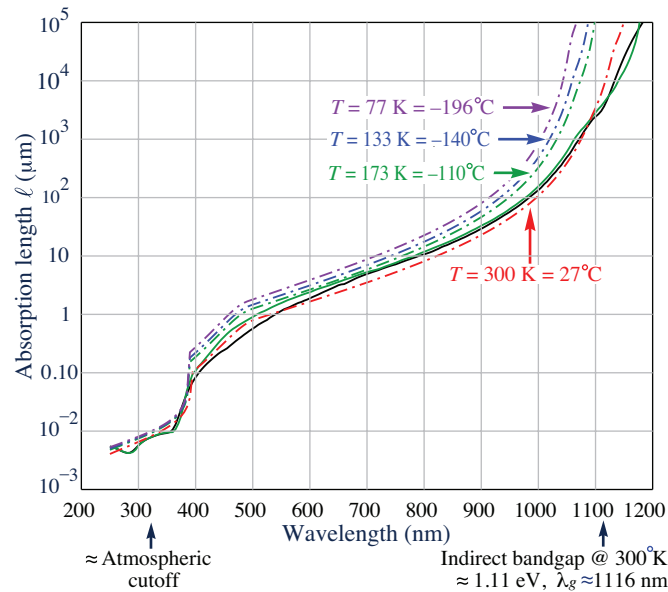


FIG. 2. The absorption length  $\ell$  in silicon<sup>a</sup>. The 300° K solid curves are from the *Handbook of Optical Constants of Solids*[4] extended to 1200 nm[5] (black) and Green[6] (gray or green). The dashed curves are calculated from the phenomenological fits by Rajkaran *et al.*[7].

<sup>a</sup> The imaginary part of the index  $k$ , absorption coefficient  $\alpha$ , and absorption length  $\ell$  are related by

$$4\pi k/\lambda = \alpha = 1/\ell.$$

1. Many sources do not consider absorption—after all, one tries to make optical coatings out of transparent materials. But once it is introduced, there is a sign ambiguity in the definition of the complex index of refraction:  $n_c = n + ik$  or  $n_c = n - ik$ . The choice is arbitrary: The positive convention is used in Refs. 9–13, while the negative convention is used in Refs. 8, 14,

and 15. Having chosen the sign, one must take care that the rest of the formalism ensures that light is attenuated in absorptive layers. *We adopt the negative sign convention.*

2. The silicon substrate is also treated as a “thin film,” although it is opaque over much of the optical range of interest. Fringes are commonly observed near the red end of a back-illuminated CCD’s sensitivity, implying coherence over the thickness of the device and, remarkably, near-specular reflection from the front surface gate structure and mechanical substrate. For a 200  $\mu\text{m}$  thick CCD the fringe spacing at  $\lambda = 1000$  nm is only 0.7 nm, and in any case the fringes are “washed out” by a finite aperture.
3. It is useful to find absorption in the antireflective (AR) coating and, separately, in the ISDP. This is done by modifying boundary conditions, valid when the absorption length in silicon is small compared to the substrate thickness.

We assume 100% internal quantum efficiency, *i.e.*, every photon absorbed in the sensitive region produces a collected electron or hole.

Model and measurement results are discussed for three antireflective coating designs: ITO/SiO<sub>2</sub>, ITO/ZrO<sub>2</sub>/SiO<sub>2</sub>, and TiO<sub>2</sub>/SiO<sub>2</sub>.

## II. MULTILAYER REFLECTED AND TRANSMITTED AMPLITUDES AND INTENSITIES

In the simplest case, a plane wave in medium  $a$  with real index  $n_0$  (usually air or vacuum) is incident at an angle  $\theta_0$  on a film with complex index  $n_1$  and thickness  $d_1$ . It exits into medium  $b$  with index  $n_s$ . With the definition  $\gamma = (n/c) \cos \theta$  (appropriate if  $\mathbf{E}$  is parallel to the surface), the boundary conditions relate the fields at the two interfaces:

$$\begin{pmatrix} E_a \\ B_a \end{pmatrix} = \begin{pmatrix} \cos \delta_1 & \frac{i \sin \delta_1}{\gamma_1} \\ i \gamma_1 \sin \delta_1 & \cos \delta_1 \end{pmatrix} \begin{pmatrix} E_b \\ B_b \end{pmatrix} \equiv \mathcal{M}_1 \begin{pmatrix} E_b \\ B_b \end{pmatrix} \quad (1)$$

The phase lag in one traversal,  $\delta_1$ , is  $(2\pi d_1/\lambda)n_1 \cos \theta_1$ . The product  $n_1 \cos \theta_1$  can be calculated from the complex version of Snell’s law:

$$n_1 \sin \theta_1 = n_0 \sin \theta_0 \quad (2)$$

The transport matrix  $\mathcal{M}_1$  contains only variables pertaining to that layer; if the light is trans-

mitted into another film a similar matrix is introduced. For  $N$  films,

$$\begin{pmatrix} E_a \\ B_a \end{pmatrix} = \mathcal{M}_1 \mathcal{M}_2 \dots \mathcal{M}_N \begin{pmatrix} E_b \\ B_b \end{pmatrix} \equiv \mathcal{M} \begin{pmatrix} E_b \\ B_b \end{pmatrix}. \quad (3)$$

The reflected fraction of the light  $r$  and the transmitted fraction  $t$  can be extracted from the boundary condition equations,

$$r = \frac{\gamma_0(m_{11} + \gamma_s m_{12}) - (m_{21} + \gamma_s m_{22})}{\gamma_0(m_{11} + \gamma_s m_{12}) + (m_{21} + \gamma_s m_{22})} \quad (4a)$$

$$t = \frac{2\gamma_0}{\gamma_0(m_{11} + \gamma_s m_{12}) + (m_{21} + \gamma_s m_{22})}, \quad (4b)$$

where the  $m_{ij}$  are the components of the product matrix  $\mathcal{M}$ .

Over most of the spectral region of interest, the silicon substrate is essentially opaque. More specifically,  $\sin \delta$  and  $\cos \delta$  both contain potentially large factors  $\exp(2\pi d|k|/\lambda)$ . While it is easy to block numerical overflows, we have found it convenient to factor out the divergent behavior:

$$\mathcal{M}_j = e^{-\delta_{Ij}} \mathcal{M}_j^F \quad (5)$$

Here  $\delta_{Ij}$  is the imaginary part of  $\delta_I$ , and, because of our negative sign convention for the imaginary part of indices, it is always negative. Eqs. (4) become

$$r = \frac{\gamma_0(m_{11}^F + \gamma_s m_{12}^F) - (m_{21}^F + \gamma_s m_{22}^F)}{\gamma_0(m_{11}^F + \gamma_s m_{12}^F) + (m_{21}^F + \gamma_s m_{22}^F)} \quad (6a)$$

$$t = \frac{2\gamma_0 \exp(\sum \delta_{Ij})}{(\gamma_0 m_{11}^F + \gamma_0 \gamma_s m_{12}^F) + (m_{21}^F + \gamma_s m_{22}^F)}. \quad (6b)$$

Since the exponential factors cancel in Eq. (6a), the reflected amplitude  $r$  is calculable for any amount of absorption, while the transmitted amplitude  $t$  is (essentially) zero for high absorption.

If  $\mathbf{B}$  is parallel to the surface, then  $\gamma = (n/c)/\cos \theta$ . Since the phase lag  $\delta$  is geometrical, it is not affected by polarization. However, in Eqs. (4b) and (6b),  $\gamma_0 (= (n_0/c) \cos \theta_0)$  in the numerator is replaced by  $(n_0/c)/\cos \theta_s$ .

The fractional reflected intensity  $R$  is  $|r|^2$ . The fractional intensity of the light transmitted into the mechanical substrate is

$$T = \frac{\Re(n_s \cos \theta_s)}{n_0 \cos \theta_0} |t|^2. \quad (7)$$

This fraction is not *per se* interesting, but if a fraction  $A$  of the light is absorbed in intermediate layers, then  $A = 1 - R - T$ . This is the QE of the CCD plus  $A_{\text{coat}}$ , the fraction of the light absorbed in the surface films including the ISDP.

The desired result, the QE, is the absorbed fraction in the substrate alone. It is necessary to separate absorption in the substrate from absorption in the complete coating and to separate absorption in the ISDP from (possible) absorption in the AR layers.

We can rewrite Eq. (3) as

$$\begin{pmatrix} E_a \\ B_a \end{pmatrix} = \mathcal{M}_{\text{AR}}\mathcal{M}_{\text{ISDP}}\mathcal{M}_{\text{Si}} \begin{pmatrix} E_b \\ B_b \end{pmatrix} \equiv \mathcal{M}_{\text{coat}}\mathcal{M}_{\text{Si}} \begin{pmatrix} E_b \\ B_b \end{pmatrix}, \quad (8)$$

where  $\mathcal{M}_{\text{AR}}$  is the product of the transfer matrices for the AR coating films,  $\mathcal{M}_{\text{ISDP}}$  is the transfer matrix for the ISDP coating,  $\mathcal{M}_{\text{Si}}$  is the matrix for the silicon substrate, and  $\mathcal{M}_{\text{coat}} = \mathcal{M}_{\text{AR}}\mathcal{M}_{\text{ISDP}}$ .

One wishes to “get inside the device” and sample the fields just after the light exits the AR coating, or after exiting the AR + ISDP coatings. Unfortunately, light is reflected back into the AR coating at the substrate interface, and we have not found an algebraic solution for the fields after the AR layers or after the AR layers plus the ISDP coating. However, an alternative method is quite accurate over almost the entire spectral region. It depends on two features of the problem:

1. Since no light is transmitted over most of the wavelength region ( $\lambda \lesssim 900$  nm, depending on the CCD thickness), we can replace the device with just the surface layers on a semi-infinite silicon substrate, and via Eqs. (4) or (6) find the fraction of the light transmitted ( $T_{\text{coat}}$ ) and reflected ( $R_{\text{coat}}$ ) by the ISDP + AR layers alone:

$$\begin{pmatrix} E_a \\ B_a \end{pmatrix} = \mathcal{M}_{\text{AR}}\mathcal{M}_{\text{ISDP}} \begin{pmatrix} E_b \\ B_b \end{pmatrix} \equiv \mathcal{M}_{\text{coat}} \begin{pmatrix} E_b \\ B_b \end{pmatrix} \quad (9)$$

Then the fraction of light absorbed by the ISDP plus AR layers ( $A_{\text{coat}}$ ) is  $1 - R_{\text{coat}} - T_{\text{coat}}$ . This can be subtracted from the absorption in the complete device to find the QE:

$$\text{QE} = A - A_{\text{coat}} \quad (10)$$

This is exact over most of the CCD, where the absorption length is small compared with the substrate thickness.

2. No serious error is introduced by lumping the Si and ISDP together as the semi-infinite silicon substrate, then calculating the transmission and reflectivity of the AR films alone. The index difference between Si and the ISDP is very small: The reflectivity is  $<0.04\%$  for  $\lambda \gtrsim 400$  nm and  $< 0.01\%$  for  $\lambda \gtrsim 650$  nm. One thus obtains  $A_{\text{AR}}$ , the intensity fraction absorbed by the AR coating alone, essentially by the ITO. Then  $A_{\text{ISDP}} = A_{\text{coat}} - A_{\text{AR}}$ .

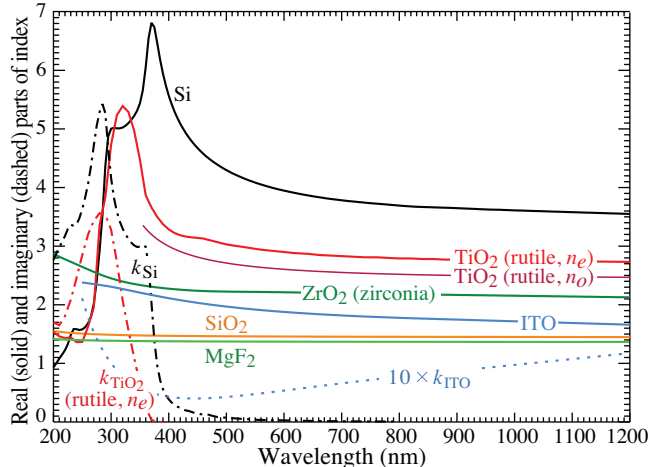


FIG. 3. Real and imaginary parts of the refractive indices of silicon and a few antireflective (AR) coating candidates. These are for bulk samples, and may not be realizable in sputtered or vapor deposited films. The ITO data are from SOPRA/ITO2.NK[16] and are significantly different from those used in our earlier work[3].

### III. REFRACTIVE INDICES

The indices of silicon and some candidate AR films are shown in Fig. 3. Indices of the transparent films ( $\text{TiO}_2$ ,  $\text{ZrO}_2$ ,  $\text{HfO}_2$ , fused  $\text{SiO}_2$ ,  $\text{MgF}_2$ , etc.) are widely tabulated for bulk samples[16], but must be used with caution, especially for sputtered or vapor-deposited films. For our application  $\text{HfO}_2$  is inferior to  $\text{ZrO}_2$ .  $\text{SiO}_2$  and  $\text{MgF}_2$  have very similar properties, but since the LBNL MicroSystems Lab has wide experience with  $\text{SiO}_2$  films, it is used in preference to  $\text{MgF}_2$ . With the exception of  $\text{SiO}_2$ , Si, ISDP, and all of the AR films used present special problems that are discussed here.

More extensive studies of candidate materials have been published by Smith & Baumeister[17] and by Lesser[18], focussing on UV transparent oxides and fluorides.

#### A. Index of silicon

While the coatings and boundary conditions at the surfaces of the CCD affect transmission and reflection, it is absorption in the silicon substrate that results in charge collection. Understanding  $k(T, \lambda)$  is therefore of paramount importance in understanding its QE. This is particularly true in the near infrared, where the absorption length  $\ell$  ( $= 1/\alpha = \lambda/4\pi k$ ) rapidly approaches the thickness of the silicon substrate as the indirect bandgap is approached (at 1.12 eV, or 1100 nm,

depending on temperature), reducing the QE to nearly zero.

Many papers over the last 60 years have been devoted to the refractive index of silicon, particularly the absorptive part, because of its great importance in solar cell design. A subset of these studies is particularly relevant to the optical and near-IR response of a CCD[6, 7, 19–28]. Two of these are relevant to our studies:

1. Green[6] (2008) published tables of optical parameters at 300° K, together with empirical power-law temperature coefficients for  $\alpha$ ,  $n$ , and  $k$ [29]: “The self-consistent tabulation was derived from Kramers-Kronig analysis of updated reflectance data deduced from the literature.” Our earlier work[3] used values of  $n$  from the *Handbook of Optical Constants of Solids*[4] extended to 1100 nm via tables presented by Janesick[5]. Green’s values are quite close to these, but in our view supersede them.

Temperature coefficients “calculated from cited and additional data sets” describe simple power laws as given in his Eqs. (9) and (10). Calculations using these coefficients indicate that the real part of the index varies only weakly with temperature. Changes are most evident near 380 nm. Since Green’s  $n(300^\circ\text{K})$  and  $n(133^\circ\text{K})$  are nearly indistinguishable, we have adopted Green’s  $n(300^\circ\text{K})$  for model calculations at all temperatures.

Absorption calculated using his coefficients yields model QE’s seriously at variance with our data. An example is shown in Fig. 11.

2. Rajkanan *et al.*[7] (1979) developed a physics-based model of the absorption that used experimental data from MacFarlane *et al.*[19] and unpublished NASA sources to determine model parameters[30]. The best accuracy was obtained “with indirect band gaps at 1.1557 and 2.5 eV and a direct allowed gap at 3.2 eV” (390 nm).

A fairly abrupt change in the absorption coefficient as the photon energy crosses this threshold (which increases somewhat with temperature) is evident in Fig. 2. Although their paper implies only 20% accuracy, we find remarkable agreement between the model predictions and our measured CCD QE at different temperatures and substrate thicknesses. At wavelengths below 390 nm, the Rajkanan *et al.* curves differ somewhat from measured values. This is due to the simple, smooth curve for  $k$  obtained from the Rajkanan *et al.* model in the direct bandgap region. It makes little practical difference, since (a) our QE measurements extend down only to 320 nm, and (b) absorptions lengths are so short (a few 10’s of nm) that the ISDP layer already confuses the issue.



Satisfactory agreement between QE modeled using the Rajhanan *et al.*'s absorption coefficient[7] and data is obtained in all cases for the fiducial region in which the QE drops from 90% to 20% of its maximum, spanning a CCD thickness range from 200  $\mu\text{m}$  to 500  $\mu\text{m}$  and temperature range from 20° C to  $-140^\circ$  C. A surprising low-energy “skirt” at the higher temperatures extending the QE well above the indirect bandgap energy is discussed in connection with the  $\text{TiO}_2/\text{SiO}_2$  coated CCD's.

### B. Index of *in-situ* doped polysilicon (ISDP)

During fabrication, a fairly thick layer of phosphorus-doped polycrystalline silicon on the rear surface of the CCD acts as an active getter, maintaining the necessary very low leakage currents through high-temperature processing steps. After thinning and polishing a backside ohmic contact is formed by depositing a thin ISDP layer (10–25 nm). The process is described in more detail in Ref. 1. Also shown in that paper is a secondary ion mass spectroscopy depth profile of a nominal 20 nm thick ISDP layer. The P concentration varies by a factor of three until a depth of 20 nm is reached, then drops exponentially at about one decade/7 nm. It is difficult to convert this profile to a single number for model calculations. In most cases the model thickness needs to be increased by 5–10 nm from the nominal value to obtain agreement with measurements.

The real part of its index is about the same as that of silicon, but it is considerably more absorptive than silicon in the blue[31]. Tables SIPOLYM.NK in the SOPRA database[16] provide  $n$  and  $k$  for  $M = 10\text{--}90$ . The peak values of both  $n$  and  $k$  decrease as  $M$  increases. Documentation of the SOPRA tables is not available, but it is likely that  $M$  is the fraction (in %) of amorphous silicon present. For  $\lambda > 450$  nm  $n$  rises slightly with  $M$ , while  $k$  increases significantly.

Holland, Wang, and Moses fabricated and measured the QE of a series of photodiodes with successively thicker ISDP coatings[32]. A sample of their data together with model fits using SIPOLY10.NK are shown in Fig. 4 for ISDP thicknesses of 10, 30, and 100 nm. In the 10 nm case the data and model are in essential agreement above 390 nm. The agreement is worse for the 30 and 100 nm cases, but the disagreement is in different directions. In all cases, and in our CCD QE measurements, the model QE falls below data for  $\lambda \lesssim 380$  nm; our assumed index is simply too absorptive in this region. Since the QE is already falling rapidly here, the error is of little practical consequence.

In the model QE calculations, ISDP absorption peaks at about 350 nm, and falls to insignificance in the red. Since there are yield concerns if the ISDP is too thin, most recent CCD's use 25 nm

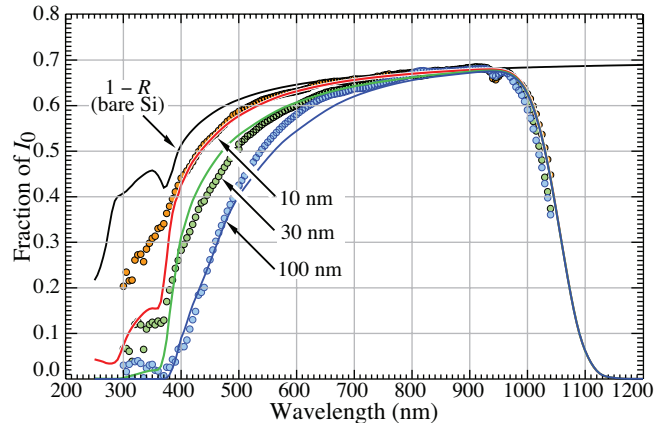


FIG. 4. Quantum efficiency of bare silicon with ISDP coatings 10, 30, and 100 nm thick. Measurements were made at “room temperature,” and the model calculations, using indices from the SOPRA SIPOLY10.NK table, were at 300° K.

coatings at the expense of significant QE loss below 500 nm.

### C. Index of indium-tin oxide (ITO)

ITO films are (nearly) transparent to visible and near-IR light. In spite of ITO’s widespread use, it is not an optically invariant material. Its optical properties depend upon the method of application, temperature, pressure, sputtering atmosphere and power, composition, and annealing. It varies from amorphous to crystalline, and often has a graded index[33–37].

ITO was first used in our application to augment rear surface conductivity and also, with careful thickness choice, to act as an AR coating or first layer of an AR coating[32]. It was reactively sputtered at room temperature in a low-pressure  $O_2/Ar$  atmosphere from a target composed of 90%  $In_2O_3$  and 10%  $SnO_2$  by weight. To optimize conduction in the ITO, the oxygen content of the film (less than saturated) was controlled using deposition parameters described in Ref. 32. Annealing in  $N_2$  for an hour at 200° C substantially improved the transmittance.

Our original sources of information about the optical constants for indium-tin oxide were the papers by Woollam, McGahan, & Johs[33] and Gerfin & Grätzel[34]. Reference 34 gives tables of 6-parameter fits to a dispersion formula for the dielectric constant  $\epsilon$ . Figure 5 shows the index, calculated as the real part of  $\sqrt{\epsilon\mu_0}/c$ , for three ITO films obtained from different sources. The Gerfin & Grätzel fits are based on data for  $350 < \lambda < 690$  nm. Data from a figure in Ref. 33 as smoothed by Gerfin & Grätzel’s dispersion formula are shown by the dash-dotted red lines, the basis of our modeling calculations until recently. The curvature change and decrease of the

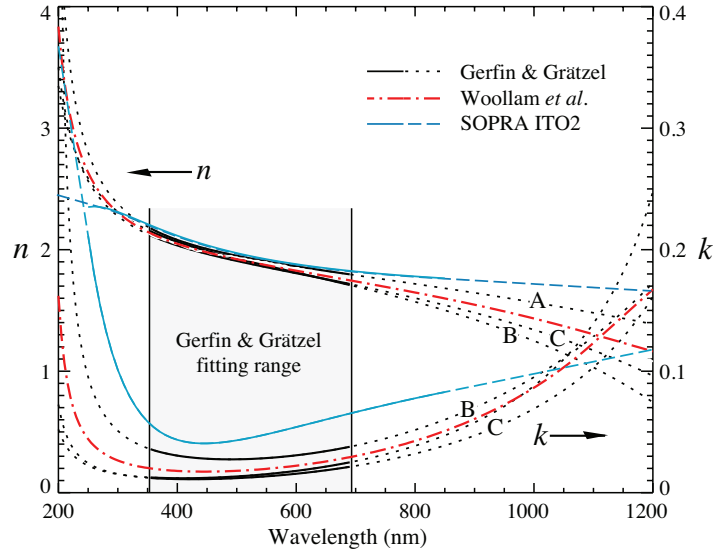


FIG. 5. Black curves show phenomenological fits to Gerfin & Grätzel’s[34] spectroscopic ellipsometric measurements of ITO indices for samples A, B, and C between 1.8 and 3.5 eV ( $\lambda\lambda = 689\text{--}354$  nm). Dotted extrapolations were made using their dispersion formula. The dash-dotted red curves are functions of the same form drawn through the measurements by Woollam *et al.*[33]. Solid magenta curves are the ITO2 indices from the SOPRA database (250–850 nm), with dashed linear extrapolations to 200–1200 nm.

index above 700 nm are expected from Drude-type absorption, indicating free carriers in the film. The solid magenta curves 250–850 nm are from ITO2.NK in the SOPRA database. The SOPRA indices, linearly extrapolated to  $\lambda = 1200$  nm, have been used recently, and provide somewhat better agreement with the measured QE. Since the dispersion fits show increasing slope of  $k$  with  $\lambda$  and decreasing slope of  $n$  with  $\lambda$ , the SOPRA data and in particular our linear extrapolation may be unphysical. Attempts to fit a Gerfin & Grätzel-style dispersion function to the SOPRA data have failed to converge. Index uncertainties in the extrapolated region are relatively unimportant in our application.

#### D. Index of zirconium oxide

The refractive index of  $\text{ZrO}_2$  from three sources is shown in Fig. 6. The SOPRA data[16] show a curious inflection at about 600 nm, perhaps from combining indices from different sources. The LBNL MicroSystems Lab (MSL) sputtered film spectroscopic ellipsometer measurements were made at the LBNL Molecular Foundry. The cubic zirconia sample measured by Wood & Nassau[38] contained 12-mole % yttria. Since the index of  $\text{Y}_2\text{O}_5$  is considerably lower than that of  $\text{ZrO}_2$ [39], one might expect the Wood & Nassau sample to have a smaller index than pure  $\text{ZrO}_2$ , as the figure

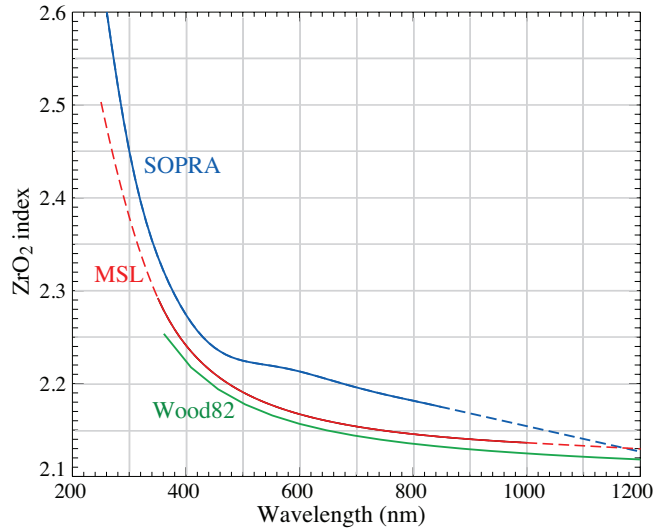


FIG. 6. The upper (blue) curve is the  $\text{ZrO}_2$  index of refraction as given in the SOPRA database (ZRO2.NK)[16]. The index shown in red (MSL, LBNL MicroSystems Lab) is from spectroscopic ellipsometer measurements made at the LBNL Molecular Foundry. The lower (green) curve is from Wood & Nassau (1982)[38]; their sample contained 12-mol % yttria. Dashed curve segments indicate extrapolations.

suggests.

The MSL and Wood & Nassau curves have roughly the same smooth shape, without the unexpected structure near 600 nm. We use the MSL index for our calculations.

### E. Index of titanium dioxide

The index of the rutile form of  $\text{TiO}_2$  shown in Fig. 3 (highest curve) is from SOPRA TIO2.NK, and tables are available through Filmetrics[16]. It may have the highest index for any transparent AR film candidate. Its wavelength dependence is remarkably similar to that of silicon, making it the near-ideal material for a wideband antireflective coating. But there are problems: the SOPRA TIO2.NK index is evidently for the extraordinary ray in this birefringent material[4, 40]. Moreover, reactively sputtered  $\text{TiO}_2$  films at temperatures consistent with CCD fabrication are mostly the (also birefringent) anatase form: “Annealing of the films in air at 850 °C showed that anatase-rutile transformation strongly depends on the deposition temperature; the films deposited at temperature below 400°C were converted to the anatase-rutile mixture films, and the films deposited at 400°C to complete rutile films”[41]. The index of anatase is considerably below that of rutile, and tables are not readily available. The many papers on the subject do not present consistent results[42–46]. For example, Dakka *et al.*[42] show different indices for “new target” (NT) and “used target”

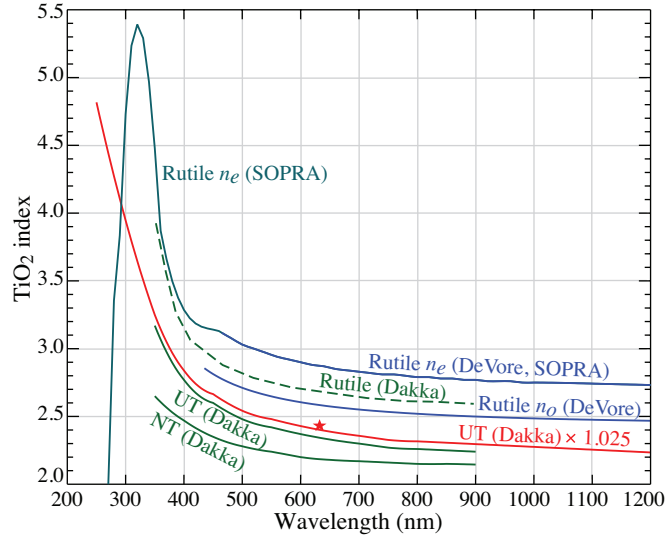


FIG. 7.  $\text{TiO}_2$  refractive indices reported by Dakka *et al.*[42], DeVore[40], and SOPRA[16]. “NT” indicates “new target,” “UT” indicates “used target.” The DeVore 1951 result for  $n_e$  is evidently used in SOPRA TIO2.NK for  $\lambda > 436$  nm. The Dakka *et al.* UT result, extrapolated and scaled by 1.025 (red curve), gives the best fit to our QE data. The star indicates the measurement supplied by the manufacturer of the film, Hionix Inc.

(UT) samples, and describe porosity and voids. The Dakka *et al.* results, together together with DeVore[40] and SOPRA[16] indices, are shown in Fig. 7.

#### F. “Index” of the mechanical substrate

When transmission becomes important in the near IR ( $\gtrsim 900$  nm, depending on the thickness of the silicon), the light exits into the gate structure and a mechanical substrate, which we have often modeled as exit into air:  $n_s = 1.0$ . It is considerably more complicated than this, as shown in Fig. 1. The light encounters 50 nm of  $\text{SiO}_2$ , then 50 nm of  $\text{Si}_3\text{N}_4$ , polysilicon gates 300 nm thick (with 40% overlap), a thick layer of  $\text{SiO}_2$ , and epoxy that binds the device to thick silicon or aluminum nitride. Remarkably, a single index  $n_s$  seems to describe this region adequately. Modeled QE turns out to be very insensitive to its value:  $n_s = 1.5$  or even  $n_s = 2.0$  moves the model calculation in the steep IR falloff region only slightly to the left, where it agrees slightly better with the measurements. However, asymptotic  $1-R$  and  $T$  increase significantly with increasing  $n_s$ . Examples are shown below for both  $n_s = 1.0$  and  $n_s = 1.5$ .

#### IV. MODEL CALCULATIONS COMPARED WITH QE AND REFLECTIVITY MEASUREMENTS

Only the reflectivity  $R$  and the transmittivity  $T$  are directly modeled. As per the discussion of Sec. II,  $1 - R - T$  can be approximately decomposed into the QE, the light fraction absorbed in the ISDP layer ( $A_{\text{ISDP}}$ ), and the fraction absorbed in the antireflective coatings ( $A_{\text{AR}}$ ). If the AR coating is not significantly absorptive, the QE and  $1 - R$  curves should be nearly identical for a fairly wide region in the red and near IR, where there is no transmission and the ISDP is essentially transparent. If the AR coating does absorb significantly at all wavelengths, then there is a calculable gap between the QE and  $1 - R$  curves, as is evident in Figs. 9 and 10. The measured QE is subject to amplifier gain uncertainties and other problems at the few-percent level. The absolute measurement of  $R$  is used to normalize the QE measurements.

The QE can be measured in either the normal CCD mode or by reading out the entire or a masked subsection of the CCD as a photodiode (PD mode). This provides some additional redundancy, and measurements can be made at higher temperatures than are possible in the CCD mode. An example is discussed in Sec. IV D.

Our setup for measuring the QE[47] is fairly standard: light from a monochromator enters an integrating sphere and exits a large aperture. It arrives at the dewar containing the CCD after an 0.8 m drift space in a baffled box. Slit widths are varied with light intensity; the bandwidth can be as small as 10 nm. A room-temperature standard photodiode at the CCD's position and behind the same dewar window is used to calibrate a similar photodiode at a small port in the integrating sphere that is then used as the reference for the QE measurement.

The reflectometer is described in Ref. 48. The intensity of a light beam from the monochromator is measured by a photodiode after several mirror reflections. One mirror is then moved so that a reflection from the (air-backed) CCD wafer sample is included in the optical path. The ratio yields the absolute reflectivity  $R$ . These measurements are at room temperature.

The CCD's have from 4 to 16 readout amplifiers whose gain calibrations can be uncertain at the few percent level. In a broad red spectral band the QE should be nearly  $1 - R$ ; this is used to normalize the QE measurements.

The CCD's fabricated and studied so far use various combinations of ISDP, ITO,  $\text{ZrO}_2$ ,  $\text{TiO}_2$ , and  $\text{SiO}_2$  films on the silicon substrate. While the index of  $\text{SiO}_2$  is very well known, the others all require special attention. In particular, the near IR response of the CCD depends crucially on the absorption coefficient of silicon, which is discussed in detail.

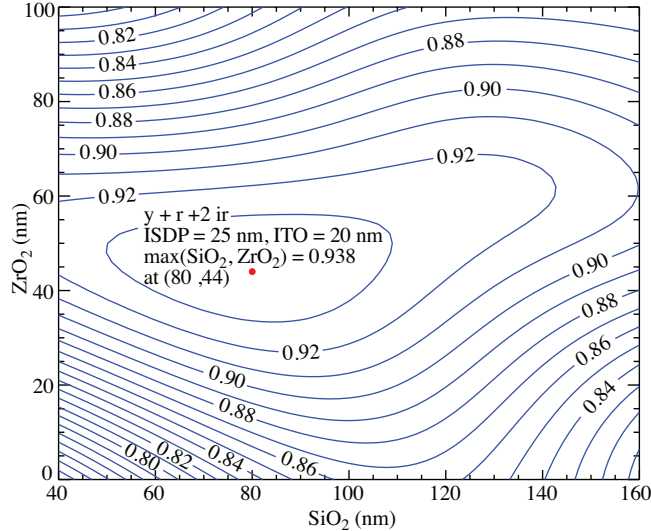


FIG. 8. Model QE contours as a function of ZrO<sub>2</sub> and SiO<sub>2</sub> thicknesses, where the QE is the average response of Hyper-Supreme-Cam  $g$  and  $i$  filters[49]. The maximum shown, at ISDP:ITO:ZrO<sub>2</sub>:SiO<sub>2</sub> = 10:20:106:42 nm, is close to the values chosen for the DESI CCD’s. The maximum of the model QE maximum using these values is 96.9% at 875 nm.

### A. Two-layer AR coating design methodology

Recent designs use a minimal-thickness ITO coating over the ISDP, followed by high-index and low-index layers. Although this is technically a 3-layer AR coating, the thickness of the ITO is held constant in optimizing the other thicknesses for maximum response.

In the absence of any clear criterion for AR coating optimization, the response was maximized for several linear combinations of broadband and narrowband filter responses. Figure 8 shows an example for an ITO (fixed 20 nm thick)/ZrO<sub>2</sub>/SiO<sub>2</sub> coating, where the model QE is the average of HSC- $g$  and HSC- $i$  responses[49]. Response was calculated for a matrix of ZrO<sub>2</sub> and SiO<sub>2</sub> thicknesses to make the QE contour plot. Thickness tolerances can be estimated from the “flatness” of the peak.

Although still somewhat subjective, the method has been moderately successful. Subsequent thickness tuning on the basis of experiment has also been useful. One problem, still not understood, is a discrepancy of 10–15% between the deposited SiO<sub>2</sub> thickness and the modeled thickness—the CCD behaves as though excessive SiO<sub>2</sub> has been deposited[50]. We correct for this empirically by depositing a thinner SiO<sub>2</sub> layer.

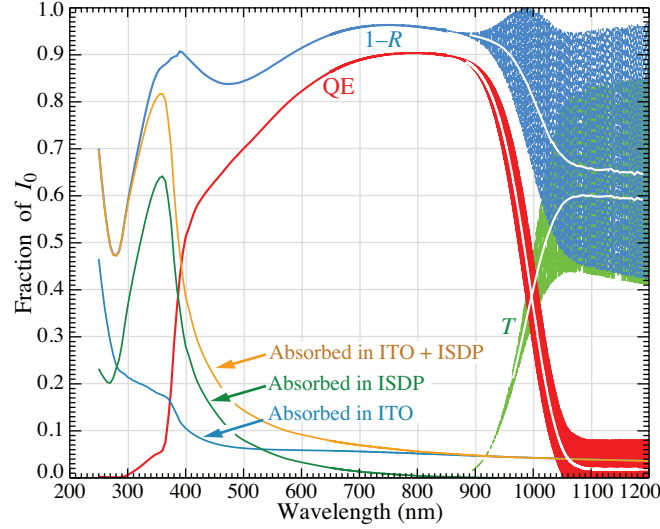


FIG. 9. Model calculation for a  $200 \mu\text{m}$  thick CCD at  $-140^\circ \text{C}$  with  $80 \text{ nm}$   $\text{SiO}_2$  and a  $58 \text{ nm}$  ITO AR coating. The ISDP layer is  $25 \text{ nm}$  thick. The differences between the QE and  $1-R$  at  $\approx 800 \text{ nm}$  and between the asymptotic  $T$  and  $1-R$  are due to absorption in the ITO. Boxcar averages over the fringe bands are indicated by the white curves. Here and in Fig. 10 the mechanical substrate index was taken as 1.0. The approximations made in calculating coating absorption break down when there is appreciable transmission, producing the spurious “foot” of the QE for  $\lambda \gtrsim 1100 \text{ nm}$ .

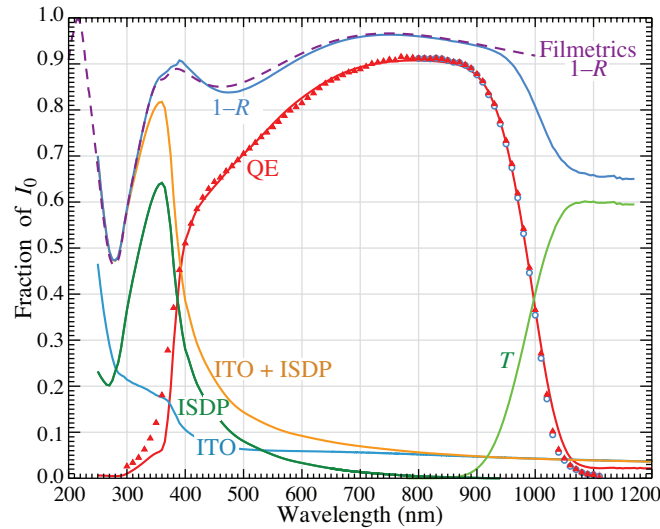


FIG. 10. Same as Fig. 9 with fringe bands removed and QE measurements added. The blue circles on the descending part of the curve indicate the measured values corrected for the monochromator bandwidth. The dashed  $1-R$  curve is from the online Filmetrics Reflectance Calculator[16].



### B. ITO/SiO<sub>2</sub> coating

In initial designs, indium-tin oxide was used both to ensure adequate rear-surface conductivity and to serve as the first layer of the AR coating. The model output is shown in Figs. 9, 10, and 13. The full calculation is shown in Fig. 9. In this and in most other examples, light is normally incident on the CCD. The decomposition of the absorption into QE, absorption in the ISDP+AR coating, ISDP, and AR is discussed in Sec. II. Above 900 nm the CCD becomes increasingly transparent, resulting in interference between the reflected and transmitted amplitudes in the silicon substrate. The responses change rapidly with increasing wavelength, and appear as bands in Fig. 9. White lines show box-car averaged  $T$ ,  $1-R$ , and QE, the intensity fraction absorbed in the sensitive region. The discrepancy between  $1-R$  and the QE in the near-IR is primarily caused by absorption in the ITO. The approximations made in separating the QE and absorption in the ISDP and ITO break down as fringing becomes more pronounced, so the modeled QE does not quite go to zero at long wavelengths.

Figure 10 shows the same curves, but with the fringing bands replaced by boxcar averages, experimental QE measurements (red triangles) added, and a dashed curve comparing the modeled  $1-R$  with results from the Filmetrics Reflectivity Calculator[16] has been added. Blue circles on the descending part of the QE response illustrate a correction for the finite monochromator bandpass.

For this model calculation  $n_s$ , the effective index of the mechanical substrate,  $n_s$ , was taken as 1.00. The value is relevant only in the transparency region,  $\lambda \gtrsim 900$  nm.

CCD's with this coating have been used in the BOSS[51] camera, in DECam[52], in the red leg of the KECK Low Resolution Spectrometer[53], and in other applications.

### C. (ITO)/ZrO<sub>2</sub>/SiO<sub>2</sub> coating

A design has been developed for the Dark Energy Spectroscopic Instrument (DESI)[54] that uses ZrO<sub>2</sub> rather than ITO for most of the high-index layer. There is a 20–25 nm ITO film between the ISDP and ZrO<sub>2</sub>. The ITO is included to avoid direct contact with a new material that might introduce reliability issues. (We have had substantial experience with ITO in direct contact with ISDP.) In any case, the ITO does not seriously compromise the QE in the DESI red and IR channels[54]. An example is shown in Fig. 11. Compared with the ITO/SiO<sub>2</sub> response (Figs. 9 and 10), the blue QE is increased and flattened, and the QE is only slightly below the  $1-R$  limit in a

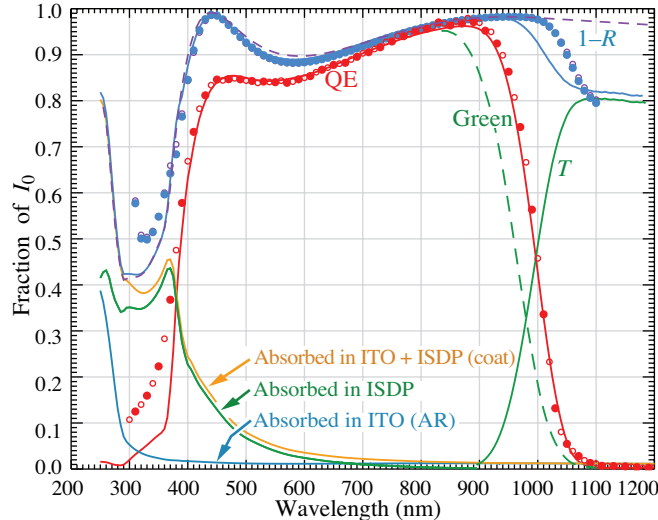


FIG. 11. The nominal ISDP:ITO:ZrO<sub>2</sub>:SiO<sub>2</sub> thickness were 11:20:38:106 nm, while a better fit (shown) is for thicknesses 18:20:38:118 nm. The wafer was 250  $\mu\text{m}$  thick, the temperature was  $-140^\circ\text{C}$  (model and QE data) and the mechanical substrate index  $n_s$  was 1.5. Reflectivity was measured at room temperature. Fringing bands are deleted from the figure. Curves show the model results; points show measurements. QE data for 12 channels are scaled for agreement near the model QE peak. The dashed curve is calculated using Green’s temperature coefficients[6].

broad red region.

For the model calculation shown here,  $n_s$ , the effective index of the mechanical substrate, was taken as 1.50. A comparison with Fig. 9, where it was 1.00, shows that the asymptotic transparency and  $1-R$  are both greater, although their difference (nearly the QE in this case) is almost unchanged.

The near-IR QE using Green’s  $k(\lambda, -140^\circ\text{C})$ [6] (Sec. III A) is also shown in Fig. 11. Green’s agreement with Rajkanan *et al.* is better when the comparison is made at  $T = 300^\circ\text{C}$ .

#### D. TiO<sub>2</sub>/SiO<sub>2</sub> coating

Since the LBNL MicroSystems Lab did not have a sputtering target for TiO<sub>2</sub> deposition, a TiO<sub>2</sub>/SiO<sub>2</sub> coating was applied to an otherwise-complete CCD by the Hionix corporation[55]. They reported a TiO<sub>2</sub> index of 2.44 at 633 nm. The SiO<sub>2</sub> film was about 14% thicker than requested, resulting in a QE somewhat lower than expected.

The response is shown in Fig. 12. Good fits to the measured QE were obtained using the Dakka “UT” index scaled by 1.025, in agreement with the Hionix measurement at 633 nm. This CCD

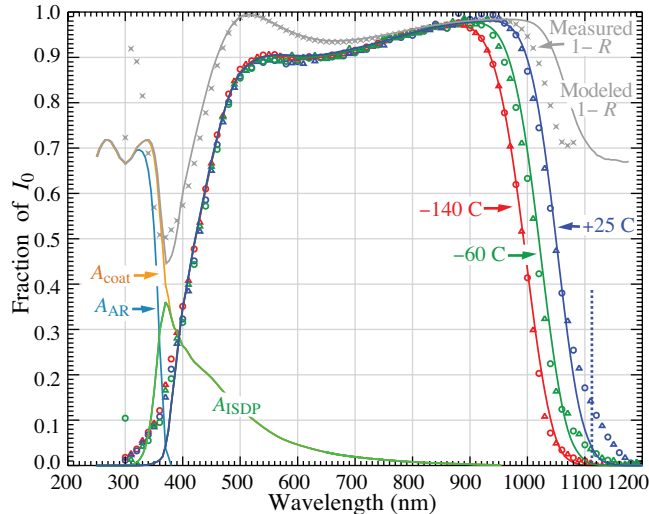


FIG. 12. Response of an ISDP/TiO<sub>2</sub>/SiO<sub>2</sub> (32 nm/57 nm/132 nm) coated CCD at  $-140$  C (CCD mode),  $-60$  C (PD mode) and  $25$  C (PD mode). Curves are the model results; points are the measurements. Substrate index is 1.5 for model QE and 1.0 for model  $1-R$ . A dotted vertical line at 1116 nm indicates the indirect bandgap at  $300^\circ$  K. At the higher temperatures, particularly at  $25$  C, the QE does not fall to zero as rapidly as the model predicts, evidently due to e-h production via a photon-two phonon processes[56].

has a better response than any of the others we have tested. Nonetheless, given the difficulty and likely unpredictability of TiO<sub>2</sub> films and only marginal improvement from the (ITO)/ZrO<sub>2</sub>/SiO<sub>2</sub> AR coating, there is little incentive to pursue this approach.

A remarkable feature of the room-temperature measurements is the QE “skirt” extending well beyond 1116 nm, the wavelength corresponding to the indirect bandgap at 1.1108 eV at  $300^\circ$  K (vertical dotted line in Fig.12). In order to conserve both energy and momentum, absorption involving indirect transitions requires the absorption or emission of one or more phonons. The Rajkanan *et al.* model[7] takes into account the two lowest phonon excitations, 0.0183 eV and 0.0577 eV that produce contributions to the absorption coefficient with displacements of  $\pm 19$  nm and  $\pm 61$  nm. As a result, the model QE at  $25^\circ$  C shown in Fig.12 is about 8% at 1100 and falls to zero by 1177 nm. However, the measured response is above 10% at 1120 nm and falls to zero only just below 1200 nm. This e-h production by low-energy photons is thought to be due to higher-temperature double-phonon processes producing offsets of  $\pm 99$  nm and  $\pm 149$  nm[19].

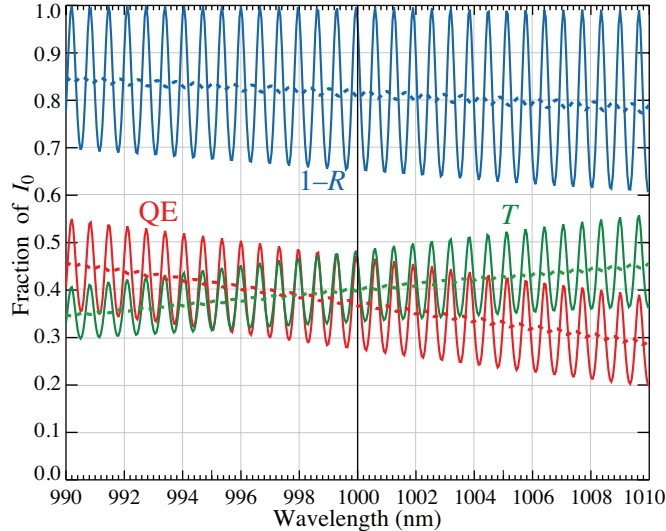


FIG. 13. Detail of the 990–1010 nm region of Fig. 9. The fringe spacing is  $\delta\lambda = \lambda^2/2nd$ , where  $d$  is the silicon thickness and  $n$  is the real part of its index (at 1000 nm,  $n = 3.57$  and  $\delta\lambda = 0.7$  nm). The dashed central curves show the results of averaging the light’s incidence angles over an f1.5 aperture. These are close to the boxcar averages, which appear to be “below center” because of the asymmetry of the Haidinger fringes.

### E. Fringing

The sensitive region of a “traditional” thin back-illuminated CCD is an epitaxial layer  $\approx 20 \mu\text{m}$  thick. At longer wavelengths light reaches the back surface, and the resulting multiple reflections produce interference “fringes.” A white-light exposure with the KECK low-resolution spectrograph (LRIS)[57] is shown in Ref. 3. The fringes are somewhat irregular because of thickness variations in the epitaxial layer, but one can infer from the fringe average spacing  $\delta\lambda$  that the layer is 20–22  $\mu\text{m}$  thick. (For a thickness  $d$  at a wavelength where the real part of the silicon index is  $n$ ,  $\delta\lambda = \lambda^2/2nd$ .) In this case, the spacing is about 7 nm at  $\lambda = 1000$  nm, providing at once a way to measure the epitaxial layer thickness[58] and a nuisance for observers. Broadband photometry using R and IR filters is plagued by swirled interference patterns whose amplitude is modulated by time-varying OH sky lines. Removal of these fringes is discussed by McLean[59] and others, and algorithms to treat the problem are part of observatory software. That the fringes exist means that the light remains coherent over at least 20  $\mu\text{m}$  and that reflection from the mechanical substrate is remarkably specular.

An expansion of our modeled 990–1100 nm region for a 200  $\mu\text{m}$  thick CCD’s is shown in Fig. 13. For normally incident light the peak-to-valley QE variation is nearly 0.2 of the incident intensity, or

0.34 of the average QE. However, the fringes are ten times closer than those in a 20  $\mu\text{m}$  thick CCD, or about 0.7 nm at 1000 nm. Only the highest-resolution spectrometers could resolve these fringes. In particular, they are not resolved in our QE measurements because of the much-wider bandpass of the monochromator. Even if they are not observed, the agreement of the boxcar averaged QE with measured QE argues for coherence and fairly specular reflection.

An actual instrument has a finite aperture, so that light arrives at different angles, each with a fringe spacing characteristic of the slant depth. The fringing pattern tends to average out. The central dashed lines in Fig. 13 were calculated for an f1.5 aperture. The remaining oscillations are the result of a beat pattern characteristic of this wavelength range; in the model they disappeared and reappeared as the aperture was changed. Results of the calculation are nearly independent of polarization.

Using a DECam CCD, Stevenson *et al.*[60] searched for water in the atmosphere of an exoplanet with the LDSS-3 spectrometer (focal ratio f2.5) at the Magellan telescope at Las Campanas Observatory. Fringes were not observed. A more detailed study of one of the images by A. Seifahrt[61] set limits on the fringe intensity of 0.25% (peak-to-valley).

DECam Y-band images have shown fringing swirls at the 0.4% peak-to-valley level[62]. The pattern and spacing is probably inconsistent with interference in the CCD itself, given its thickness and expected thickness variations. It is possible that the interference originates in the epoxy layer binding the CCD to the mechanical substrate, which was aluminum nitride for the DECam CCD's.

In any case, the steep QE falloff in the near IR limits any possible fringing to the 900–1050 nm region. The fringing amplitude, especially in the cases of the DESI (ITO)/ZrO<sub>2</sub>/SiO<sub>2</sub> CCD(Fig. 11) and the TiO<sub>2</sub>/SiO<sub>2</sub> CCD (Fig. 12), is minimized by the very low reflectivity in this region. For normally incident light the maximum peak-to-valley QE variation is 0.10 for the DESI CCD and 0.08 for the TiO<sub>2</sub>/SiO<sub>2</sub> CCD.

## V. PROSPECTS FOR QE IMPROVEMENT

It was mentioned above that the model thicknesses had to be “tuned” somewhat to obtain agreement with the measurements. To some extent this was because of variation in the actual film thicknesses, or, more likely, that the thin film indices were different from those measured in bulk samples. (In the case of TiO<sub>2</sub>, there was even ambiguity about the crystal form.) Thus by perturbing the actual film thicknesses the QE can be improved. Experimental AR coatings are being made to explore this. It is likely that response of the (ITO)/ZrO<sub>2</sub>/SiO<sub>2</sub> (DESI) CCD can be

enhanced in the 450–600 nm region from about 84% to about 90% by increasing the design  $\text{ZrO}_2$  thickness by 7–10 nm—a spectral region just below the DESI red channel, but the increased blue response might be useful for other applications.

Our blue response is limited by absorption in the ISDP rear electrode. An alternate approach is delta doping, depositing approximately a monolayer of dopant atoms on the rear surface via molecular beam epitaxy (MBE). This technique has been developed at the Jet Propulsion Lab (Caltech) for a variety of spacecraft and sounding rocket missions[63]. The object is to obtain reflection-limited ultraviolet quantum efficiency down to about 100 nm.

Antimony layers about 5 nm thick were applied in this way to 2k×4k and 1k×1k LBNL CCD’s similar to those described here[64, 65]. QE measurements with and without a (nominally)  $\text{Si}_3\text{N}_4/\text{SiO}_2$  AR coating are shown in Ref. 64. The results are consistent with ours except that their QE remains high down to about 400 nm.

There has been no further work on the delta-doping approach.

## VI. CONCLUSIONS

We have extended standard thin-film optics methods to model the quantum efficiency (QE) of LBNL thick, back-illuminated CCD’s, and compared the results with experimental measurements of QE and reflectivity for three antireflective coating examples. The calculations included (a) considering the thick substrate as one of the films and (b) separating absorption in an ISDP coating serving as the rear contact and in the antireflective coating from absorption in the silicon substrate (the QE) by modifying boundary conditions. Problems encountered with the indices involved are discussed. While agreement with experimental QE and reflectivity measurements are regarded as adequate, it is limited by uncertainties in the ISDP index, the ITO and  $\text{TiO}_2$  indices, and film deposition thickness variations. Fringing is neither expected nor observed.

## VII. ACKNOWLEDGEMENTS

The QE “machine” was built by Jens Stecker and the reflectometer by Maximilian Fabricius, both in collaboration with and under the supervision of Armin Karchar. With the exception of  $\text{TiO}_2$ , AR coatings were applied in the LBNL MicroSystems Lab. We are also grateful for Chris Bebek’s encouragement and guidance. .

This work was supported by the U.S. Department of Energy under Contract No. DE-AC02-

05CH11231.

- 
- [1] S. Holland, D. Groom, N. Palaio, R. J. Stover, and M. Wei, in *IEEE Trans. Electron Devices*, Vol. 50 (2003) pp. 225–238.
- [2] S. E. Holland, C. J. Bebek, K. S. Dawson, J. H. Emes, M. H. Fabricius, J. A. Fairfield, D. E. Groom, A. Karcher, W. F. Kolbe, N. P. Palaio, N. A. Roe, and G. Wang, in *Society of Photo-Optical Instrumentation Engineers (SPIE) Conference Series, Proc. SPIE*, Vol. 6276 (2006) p. 62760B.
- [3] D. E. Groom, S. E. Holland, M. E. Levi, N. P. Palaio, S. Perlmutter, R. J. Stover, and M. Wei, in *Sensors, Cameras, and Systems for Scientific/Industrial Applications, Proc. SPIE*, Vol. 3649, edited by M. M. Blouke and G. M. Williams (1999) pp. 80–90.
- [4] D. F. Edwards, *Handbook of Optical Constants of Solids*, edited by E. D. Palik (Academic Press, 1985) pp. 547–569.
- [5] J. R. Janesick, IS&T/SPIE Symposium on Electronic Imaging Science and Technology , 233 (no data source or year given).
- [6] M. A. Green, *Solar Energy Materials and Solar Cells* **92**, 1305 (2008).
- [7] K. Rajkanan, R. Singh, and J. Shewchun, *Solid-State Electronics* **22**, 793 (1979).
- [8] F. L. Pedrotti and L. S. Pedrotti, *Introduction to Optics* (Prentice Hall, New Jersey, 1993).
- [9] E. Hecht, *Optics*, 3rd ed. (Addison-Wesley, 1998).
- [10] H. A. Macleod, *Thin-Film Optical Filters*, 3rd ed. (Institute of Physics, Bristol, 2001).
- [11] F. A. Jenkins and H. E. White, *Fundamentals of Optics (2nd edition)* (McGraw Hill, New York, 1950).
- [12] W. K. Panofsky and M. Phillips, *Classical Electricity and Magnetism* (Addison-Wesley, Redding, MA, 1955).
- [13] J. C. Slater and N. H. Frank, *Electromagnetism* (McGraw-Hill, New York, 1947).
- [14] M. Born and E. Wolf, *Principles of Optics*, 7th ed. (Pergamon, Cambridge, 1999).
- [15] A. Sommerfeld, *Optics* (Academic Press, New York, 1964).
- [16] Most useful indices can be downloaded from [filmmetrics.com](http://filmmetrics.com). Many are from the SOPRA Material Database, given without citation. In some cases polynomial or dispersion fits can be found.
- [17] D. Smith and P. Baumeister, *Applied Optics* **18**, 111 (1979).
- [18] M. Lesser, *Optical Engineering* **26**, 911 (1987).
- [19] G. G. Macfarlane, T. P. McLean, J. E. Quarrington, and V. Roberts, *Phys. Rev.* **111**, 1245 (1958).
- [20] W. C. Dash and R. Newman, *Phys. Rev.* **99**, 1151 (1955).
- [21] H. R. Philipp and E. A. Taft, *Phys. Rev.* **120**, 37 (1960).
- [22] H. A. Weakliem and D. Redfield, *J. App. Phys.* **50**, 1491 (1979).
- [23] G. E. Jellison, Jr. and F. A. Modine, *J. App. Phys.* **53**, 3745 (1982).

- [24] G. E. Jellison, Jr. and F. A. Modine, *Appl. Phys. Lett.* **41**, 180 (1982).
- [25] G. E. Jellison, Jr. and H. H. Burke, *J. App. Phys.* **60**, 841 (1986).
- [26] G. E. Jellison, *Optical Materials* **1**, 41 (1992).
- [27] K. Bücher, J. Bruns, and H. G. Wagemann, *J. App. Phys.* **75**, 1127 (1994).
- [28] M. A. Green and M. Keevers, *Progress in Photovoltaics* **3**, 189 (1995).
- [29] To maintain the required significance at longer wavelengths it is necessary to recalculate  $k$  from Green's absorption coefficients. Tables are most easily copied from the web version: [sciencedirect.com/science/article/pii/S0927024808002158#](http://sciencedirect.com/science/article/pii/S0927024808002158#).
- [30] A nearly-identical expression for  $\alpha$  is given by Bücher *et al.*[27] without reference to Rajkanan *et al.*'s earlier paper. With two exceptions, the parameters are the same or nearly the same. However, the direct allowed bandgap contribution is given as  $A(\hbar\omega - E_{gd})^{3/2}/\hbar\omega$ , rather than Rajkanan *et al.*'s  $A(\hbar\omega - E_{gd})^{1/2}$ . Evidently the exponent should be 1/2 for a direct bandgap transition[56]. Although both forms give similar results for photon energies below  $E_{gd}$ , we choose Rajkanan *et al.*'s form.
- [31] G. Lubberts, B. C. Burkey, F. Moser, and E. A. Trabka, *J. Appl. Phys.* **52**, 6870 (1981).
- [32] S. E. Holland, N. W. Wang, and W. W. Moses, *IEEE Trans. Nucl. Sci.* **44**, 443 (1997).
- [33] J. A. Woollam, W. A. McGahan, and B. Johs, *Thin Solid Films* **241**, 44 (1994).
- [34] T. Gerfin and M. Grätzel, *J. Appl. Phys.* **79**, 1722 (1996).
- [35] S. B. Lee, J. C. Pincenti, A. Cocco, and D. L. Naylor, *J. Vac. Sci. Tech. A* **11**, 2742 (1993).
- [36] H. E. Rhaleb *et al.*, *Applied Surface Science* **201**, 138 (2002).
- [37] C. Guillén and J. Herrero, *J. App. Phys.* **101**, 073514 (2007).
- [38] D. L. Wood and K. Nassau, *Appl. Optics* **21**, 2978 (1982).
- [39] Y. Nigara, *Jpn. J. Appl. Phys.* **7**, 404 (1968).
- [40] J. R. DeVore, *J. Opt. Soc. Am.* **41**, 416 (1951).
- [41] D. Wicaksana, A. Kobayashi, and A. Kinbara, *J. Vac. Sci. Technol. A* **10**, 1479 (1992).
- [42] A. Dakka, J. Lafait, M. Abd-Lefdil, and C. Sella, *M.J.Condensed matter* **2**, 153 (1999).
- [43] H. Tang, H. Berger, P. Schmid, and F. Levy, *Solid State Communications* **92**, 267 (1994).
- [44] P. G. R. Dannenberg, *Thin Solid Films* **360**, 122 (2000).
- [45] G. E. Jellison *et al.*, *J. Appl. Phys.* **93**, 9537 (2003).
- [46] L. Miao, P. Jin, K. Kaneko, A. Terai, N. Nabatova-Gabain, and S. Tanemura, *App. Surface Sci.* **212-213**, 255 (2003).
- [47] D. E. Groom, C. J. Bebek, M. Fabricius, A. Karcher, W. F. Kolbe, N. A. Roe, and J. Steckert, in *Sensors, Cameras, and Systems for Scientific/Industrial Applications VII, Proc. SPIE*, Vol. 6068, edited by M. M. Blouke (2006) pp. 133–143.
- [48] M. H. Fabricius, C. J. Bebek, D. E. Groom, A. Karcher, and N. A. Roe, in *Sensors, Cameras, and Systems for Scientific/Industrial Applications VII, Proc. SPIE*, Vol. 6068, edited by M. M. Blouke (2006) pp. 144–154.
- [49] S. Kawanomoto *et al.*, in prep.



- [50] Blacksberg *et al.* report measured film indices somewhat different than were expected[64]. For SiO<sub>2</sub> they find a film index about 2% higher than for bulk fused quartz, in the right direction but not enough to explain our apparent excess.
- [51] S. A. Smee, J. E. Gunn, A. Uomoto, N. Roe, D. Schlegel, *et al.*, *Astron. J.* **146**, 32 (2013).
- [52] B. Flaughner, H. T. Diehl, K. Honscheid, *et al.*, *Astron. J.* **150**, 150 (2015), arXiv:1504.02900.
- [53] C. Rockosi, R. Stover, *et al.*, in *Ground-based and Airborne Instrumentation for Astronomy III*, SPIE, Vol. 7735 (2010) p. 77350R.
- [54] C. Bebek, J. Emes, D. Groom, S. Haque, S. Holland, A. Karcher, W. Kolbe, J. Lee, N. Palaio, and G. Wang, *J. Instr.* **10**, C05026 (2015).
- [55] Hionix, Inc., [hionix.com](http://hionix.com).
- [56] J. I. Pankove, *Optical processes in semiconductors* (Dover Publications, New York, 1971) pp. 36–42.
- [57] J. B. Oke *et al.*, *P. A. S. P.* **107**, 375 (1995).
- [58] J. R. Janesick, *Scientific charge-coupled devices*, Bellingham, WA: SPIE Optical Engineering Press, 2001, *xvi*, 906 p. SPIE Press monograph, PM 83 (2001).
- [59] I. S. McLean, ed., *Electronic imaging in astronomy. Detectors and instrumentation* (UK Wiley, Chichester, 1997).
- [60] K. B. Stevenson, J. L. Bean, A. Seifahrt, *et al.*, *Astrophys. J.* **817**, 141 (2016), arXiv:1511.08226.
- [61] Andreas Seifahrt (Univ. of Chicago), personal communication (2016).
- [62] P. Martini (Ohio State Univ.), personal communication (2012).
- [63] S. Nikzad, A. D. Jewell, M. E. Hoenk, T. Jones, J. Hennessy, T. Goodsall, A. Carver, C. Shapiro, S. R. Cheng, E. Hamden, G. Kyne, D. C. Martin, D. Schiminovich, P. Scowen, K. France, S. McCandliss, and R. E. Lupu, ArXiv e-prints (2016), arXiv:1612.04734 [astro-ph.IM].
- [64] J. Blacksberg, S. Nikzad, M. E. Hoenk, S. E. Holland, and W. F. Kolbe, *IEEE Transactions on Electron Devices* **55**, 3402 (2008).
- [65] B. C. Jacquot, S. P. Monacos, T. J. Jones, J. Blacksberg, M. E. Hoenk, and S. Nikzad, in *High Energy, Optical, and Infrared Detectors for Astronomy IV*, *Proc. SPIE*, Vol. 7742 (2010) p. 77420I.